INTERNATIONAL JOURNAL OF CLIMATOLOGY
Int. J. Climatol. **32**: 1226–1237 (2012)
Published online 17 May 2011 in Wiley Online Library
(wileyonlinelibrary.com) DOI: 10.1002/joc.2347

RMetS
Royal Meteorological Society

Spatial patterns and regimes of daily precipitation in Iran in relation to large-scale atmospheric circulation

Tayeb Raziei,[a]* Abbas Mofidi,[b] João A. Santos[c] and Isabella Bordi[d]

[a] *Soil Conservation and Watershed Management Research Institute (SCWMRI), Tehran, Iran*
[b] *Department of Geography, Ferdowsi University of Mashhad, Mashhad, Iran*
[c] *Centre for the Research and Technology of Agro-Environmental and Biological Sciences (CITAB), University of Trás-os-Montes and Alto Douro5001-801 Vila Real, Portugal*
[d] *Department of Physics, University of Rome "La Sapienza", Rome, Italy*

ABSTRACT: The relationships between large-scale atmospheric circulation types and seasonal regimes of daily precipitation over Iran are assessed using daily precipitation from a high-resolution gridded dataset provided by the Asian Precipitation-Highly Resolved Observational Data Integration Towards the Evaluation of Water Resources (APHRODITE) Project. Regional spatial modes of daily precipitation variability were identified by S-mode Principal Component Analysis (PCA) with Varimax rotation, applied to the subset of days when at least 10% of all grid-points over Iran received precipitation $\geq$5 mm. The study refers to the period 1961–2004 and is carried out for each season (excluding summer) separately. To characterize the dynamical features associated with each regional precipitation regime (PR), composites of daily atmospheric fields are computed by only averaging days with rotated PCA scores $\geq$1.5 (strong positive phase). In autumn and winter, Iran is divided into five PRs, while four PRs are identified in spring. Results suggest that the spatial distribution of precipitation over Iran is largely governed by the geographical position of both the mid-tropospheric trough over the Middle East and the Arabian anticyclone. In fact, in almost all PRs, the trough, as a pre-conditioning factor, leads to regional-scale ascending motions, whereas the Arabian anticyclone induces low-tropospheric moisture transports from southern water bodies into the cyclonic systems near Iran, triggering rain-generating conditions. Copyright © 2011 Royal Meteorological Society

KEY WORDS daily precipitation; atmospheric circulation types; precipitation regimes; Iran; APHRODITE

Received 6 October 2010; Revised 28 February 2011; Accepted 2 April 2011

1. Introduction

Space-time variability of precipitation in a region plays an essential role in water resource management, motivating many research efforts to identify large-scale atmospheric circulation types leading to precipitation events and their effects on the frequency and amount of precipitation (Lamb, 1977; Bogardi *et al*., 1994; Frakes and Yarnal, 1997). Many authors have studied the possible linkages between large-scale atmospheric circulation and precipitation (e.g. Corte-Real *et al*., 1998; Romero *et al*., 1999; Wibig, 1999; Xoplaki *et al*., 2000; Kidson, 2000; Santos *et al*., 2005).

Owing to the complex orography (Figure 1) and wide latitudinal extent – from the Hadley cell descending branch up to mid-latitudes – precipitation in Iran is highly variable both in space and time. Precipitation occurrences and amounts vary from the relatively humid western mountainous areas to the arid and semi-arid regions of central and eastern Iran, which are characterized by sporadic precipitation events. Additionally, the increasing water demand, due to population growth, urbanisation, and industrialisation, has further increased the vulnerability to droughts. As such, a comprehensive analysis of the relationship between precipitation regimes (PR) in Iran and large-scale atmospheric circulation is of great interest. It should be noted that the existence of such relationship is of crucial importance not only for the study area, but also for other geographical contexts, since it enables the prediction of precipitation events at regional scale given the atmospheric pre-conditioning factors. Therefore, the present study illustrates a methodology that can be easily applied in other regions with reliable precipitation datasets.

Domroes *et al*. (1998), by applying a Principal Component Analysis (PCA) and Cluster Analysis (CA) to monthly precipitation recorded at 71 stations irregularly distributed across Iran, identified 5 sub-regions with different PRs. Dinpashoh *et al*. (2004), using 77 stations throughout Iran and following a similar approach, isolated 7 climatic sub-regions. Soltani *et al*. (2007) also analysed PRs using monthly precipitation time series from 28 sites, and 3 main climatic groups were found by applying a hierarchical cluster analysis. Using a dense

* Correspondence to: Tayeb Raziei, Soil Conservation and Watershed Management Research Institute (SCWMRI), P.O. Box 13445-1136, Tehran, Iran. E-mail: tayebrazi@scwmri.ac.ir

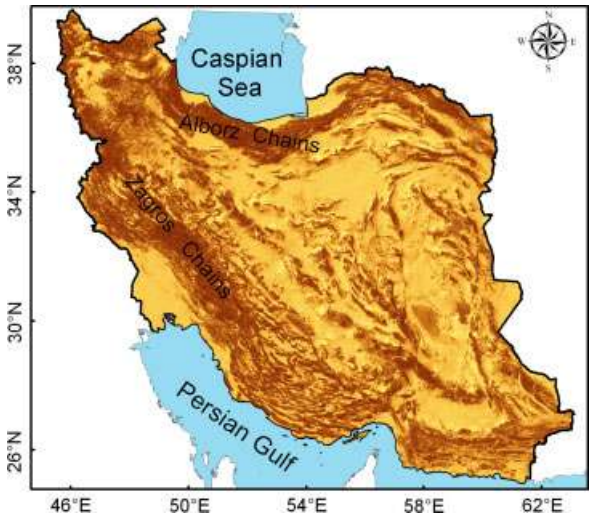

Figure 1. Topographic map of Iran. This figure is available in colour online at wileyonlinelibrary.com/journal/joc

rain-gauge network, Raziei *et al*. (2008) analysed the precipitation patterns in western Iran and divided the studied area into 5 sub-regions with different PRs.

For studying the possible linkage between large-scale teleconnection indices and surface climate variables in Iran, Ghasemi and Khalili (2008) investigated the relationship between the North Sea–Caspian Pattern (NCP) and winter temperature variability in Iran, showing that the NCP has a strong negative correlation with winter temperatures. Furthermore, it was found that the positive phase of NCP is associated with strong cyclonic activity over Iran, causing enhanced cloudy conditions and precipitation. Nazemosadat and Cordery (2000) found a negative correlation between the Southern Oscillation Index (SOI) and precipitation over most of Iran (cold phase of ENSO favours precipitation), particularly over the southern foothills of the Alborz Mountains, the northwestern and central areas. In addition, Nazemosadat and Ghasemi (2004) showed that warm ENSO events substantially reduce (increase) the intensity and probability of occurrence of dry (wet) periods during autumn, particularly over southern Iran. However, Raziei *et al*. (2009) studied the relationship between the ENSO and the hydrological drought in western Iran and concluded that there is no clear evidence for a link between them.

Alijani (2002) studied the spatial and temporal variability of 500-hPa geopotential heights and their relationship with precipitation and temperature anomalies over Iran, concluding that regional troughs/ridges lead to important winter precipitation and temperature anomalies. Recently, Raziei *et al*. (2011) objectively keyed winter mean daily 500-hPa geopotential height into 12 atmospheric circulation types (CTs) and analysed their relationship with dry/wet events in western Iran. Significant correlations between the frequencies of occurrence of CTs and of dry/wet spells were found, suggesting that particular CTs are potential predictors for winter dry/wet events in western Iran.

Owing to the coarse meteorological networks used in most of the aforementioned studies, a comprehensive analysis of precipitation in Iran using a high-resolution database is necessary. The objectives of the current study are two-fold: (1) identifying the spatial patterns of seasonal daily precipitation variability over Iran; and (2) isolating the large-scale atmospheric circulation types associated with the identified PRs in each sub-region.

2. Data and methods

2.1. Data

The availability of daily gridded precipitation from the Asian Precipitation-Highly Resolved Observational Data Integration Towards the Evaluation of Water Resources (APHRODITE) project for the Middle East (Yatagai *et al*., 2008, 2009), with the high spatial resolution of 0.5° latitude × 0.5° longitude, motivated the present study.

To develop the APHRODITE daily precipitation dataset for the Middle-East (20 °E–65 °E, 20 °N–50 °N), a total of 1394 stations (including GTS stations with only 5 or more years of records) from all countries in the domain have been used (Yatagai *et al*., 2008). Station data for Iran, Turkey, and Israel were supplied by national organisations and directly used for gridding, while for the remaining countries of the domain the same database adopted by Chen *et al*. (2002) was used. Several conventional quality control schemes have been applied to raw data (Yatagai *et al*., 2008). Gridded daily precipitation is then obtained by interpolating rain-gauge observations using a modified version of the Shepard (1968) algorithm; this algorithm takes into account not only the horizontal distance, but also local topographical features (e.g. elevation and mountain slopes). After calculating the daily precipitation climatology, the ratios of daily precipitation to the climatology are interpolated to a 0.05° grid resolution. Each daily gridded ratio is then multiplied by the corresponding climate-mean precipitation. Finally, the 0.05° gridded fields are re-gridded to 0.5° and 0.25° grids (Yatagai *et al*., 2009).

In the present study, the latest version of APHRODITE (APHRO_V0902) dataset on the 0.5° grid was used. It is based on 337 Iranian meteorological stations with minimum record length of 5 years. The rain-gauge stations are composed of 154 World Meteorological Organization (WMO) stations and of 183 non-WMO stations, spread throughout Iran and covering different temporal periods, with the longest starting in the 1960s (Yatagai *et al*., 2008). The common time period (1961–2004) is selected here. In order to identify seasonal spatial patterns of daily precipitation over Iran, only grid points representative of the country (638) have been considered for the analysis.

For studying the linkage between the identified PRs in the sub-regions and large-scale atmospheric circulation types, 500-hPa daily mean geopotential height and daily means of specific humidity, zonal (U) and meridional (V) wind components at 850 hPa and mean

sea level pressure are retrieved from the National Centers for Environmental Prediction/National Center for Atmospheric Research (NCEP/NCAR) reanalysis archive (Kistler *et al.*, 2001). All fields have a spatial resolution of 2.5° latitude × 2.5° longitude.

2.2. Principal Component Analysis

Principal Component Analysis is a multivariate statistical tool (Rencher, 1998) extensively used for analysing precipitation variability in different geographical locations (e.g. Bonell and Sumner, 1992; Esteban-Parra *et al.*, 1998; Serrano *et al.*, 1999). In this study, to indentify the seasonal spatial patterns of daily precipitation across Iran, the S-mode PCA (Richman, 1986) is applied to the subset of days when at least 10% of all grid points covering Iran (638 grid points) have precipitation totals $\geq$5 mm. The first criterion was used to exclude small-scale precipitation events, commonly generated by local convection and/or orographic mechanisms, while the second criterion was utilized to filter out short-lasting events with unimportant precipitation amounts. Hence, only events that are produced by large-scale circulation patterns are considered in the upcoming analysis.

The following seasons are taken into account: autumn, winter, and spring, defined as September–November (SON), December–February (DJF), March–May (MAM), respectively. Summer is excluded, since it is, on average, extremely dry in almost all of the country, owing to the dominant subtropical high-pressure system that induces strong subsidence and resulting stable weather conditions. In mountainous areas of western and northern Iran, as well as along the Caspian Sea coast, summer precipitation may be occasionally generated by convective and/or topographic mechanisms. It also occurs in southeastern Iran, here mainly due to the remote influence of the Asian monsoon system. Therefore, summertime precipitation tends to be sporadic and local and few summer events met the two prescribed thresholds, plainly justifying its exclusion from our analysis.

Since some assumptions in PCA require normally distributed variables (Fovell and Fovell, 1993), the log10-transformation is applied to daily precipitation prior to PCA; zero values are replaced by 0.01 before taking logarithms (Romero *et al.*, 1999; Neal and Phillips, 2009). This transformation significantly reduces the positive skewness of the empirical distributions, yielding their convergence to normality.

The initial data matrices used as inputs for PCA consist of 638 × 684, 638 × 976, 638 × 721 (variables × cases) for SON, DJF, and MAM, respectively; variables are the selected grid points over Iran (638) and cases correspond to days when at least 10% of all grid points have precipitation totals $\geq$5 mm. The highest number of cases for DJF suggests that the frequency of wide spread precipitation events in Iran is higher in winter than in spring and autumn. This can be mostly attributed to the wintertime strong large-scale circulation and to the respective precipitation maximum.

Following North's rule-of-thumb (North *et al.*, 1982), the sampling errors of the PCA eigenvalues are estimated in order to objectively define the number of orthogonal modes to be retained for Varimax rotation (non-degenerated modes). Rotation enables a statistically based climate regionalisation (Rencher, 1998) and the rotated PC scores (RPCs) represent the temporal variability of the corresponding rotated spatial mode of the precipitation variability (herein, precipitation mode).

2.3. Large-scale circulation types

In order to analyse the connection between the seasonal regimes of daily precipitation and the driving large-scale atmospheric circulation types, a compositing methodology is applied (Yarnal *et al.*, 2001). Composites of several atmospheric fields for each precipitation mode are computed by only taking into account days with RPC $\geq$1.5 (strong positive phase). A large number of days are discarded when choosing a higher value (e.g. 2.0), reducing the significance of the composites, whereas a large number of days with small and local precipitation amounts are selected when choosing a lower threshold (Kostopoulou and Jones, 2007). Composite maps of the contributions of each mode to total precipitation, of the 500-hPa geopotential height and respective relative vorticity, of the 850-hPa moisture transport and corresponding streamlines are also computed for each considered season and for each precipitation mode. These variables jointly provide a detailed description of the main dynamical features associated with a PR. Lastly, the representativeness of each composite was assessed by projecting the respective daily maps onto it.

3. Results

3.1. Seasonal spatial modes of daily precipitation variability

The S-mode PCA is applied to the log10-transformed precipitation time series for SON, DJF and MAM. According to North's rule-of-thumb, only the first 5 (4) orthogonal modes for SON and DJF (MAM) are 'well-defined' (i.e. non-degenerated) at a 95% confidence level and are then retained for subsequent rotation. Table I lists the percentages of total variance, for each season, by un-rotated and rotated modes. The first 5 (4) modes approximately represent 59% (55%) of total variance for SON and DJF (MAM), which are reasonably high percentages taking into account the complexity of daily precipitation fields in Iran.

Figure 2 displays the rotated empirical orthogonal functions (REOFs) of daily precipitation for SON, DJF, and MAM, ranked according to their similarity rather than to their eigenvalues. Figure 2(a)–(e) shows the five REOFs of daily precipitation for SON. As can be noted the country is divided into five sub-regions, each one characterized by high positive loadings (loadings represent the correlations between the log10-transformed precipitation and the corresponding RPCs). The first and

Table I. Fractions of total variance (in %) represented by the retained un-rotated and Varimax rotated EOF modes of daily precipitation in autumn (SON), winter (DJF), and spring (MAM).

Mode	SON		DJF		MAM	
	Un-rotated	Rotated	Un-rotated	Rotated	Un-rotated	Rotated
1	24.7	14	25.7	13.7	26.7	16.2
2	15.1	13.8	13.9	13.7	12.6	13.5
3	9.9	13.1	8.5	10.9	10.0	12.8
4	5.7	11.4	6.5	10.6	6.0	12.7
5	3.7	6.9	4.3	9.9		
Total	59.2	59.2	58.8	58.8	55.2	55.2

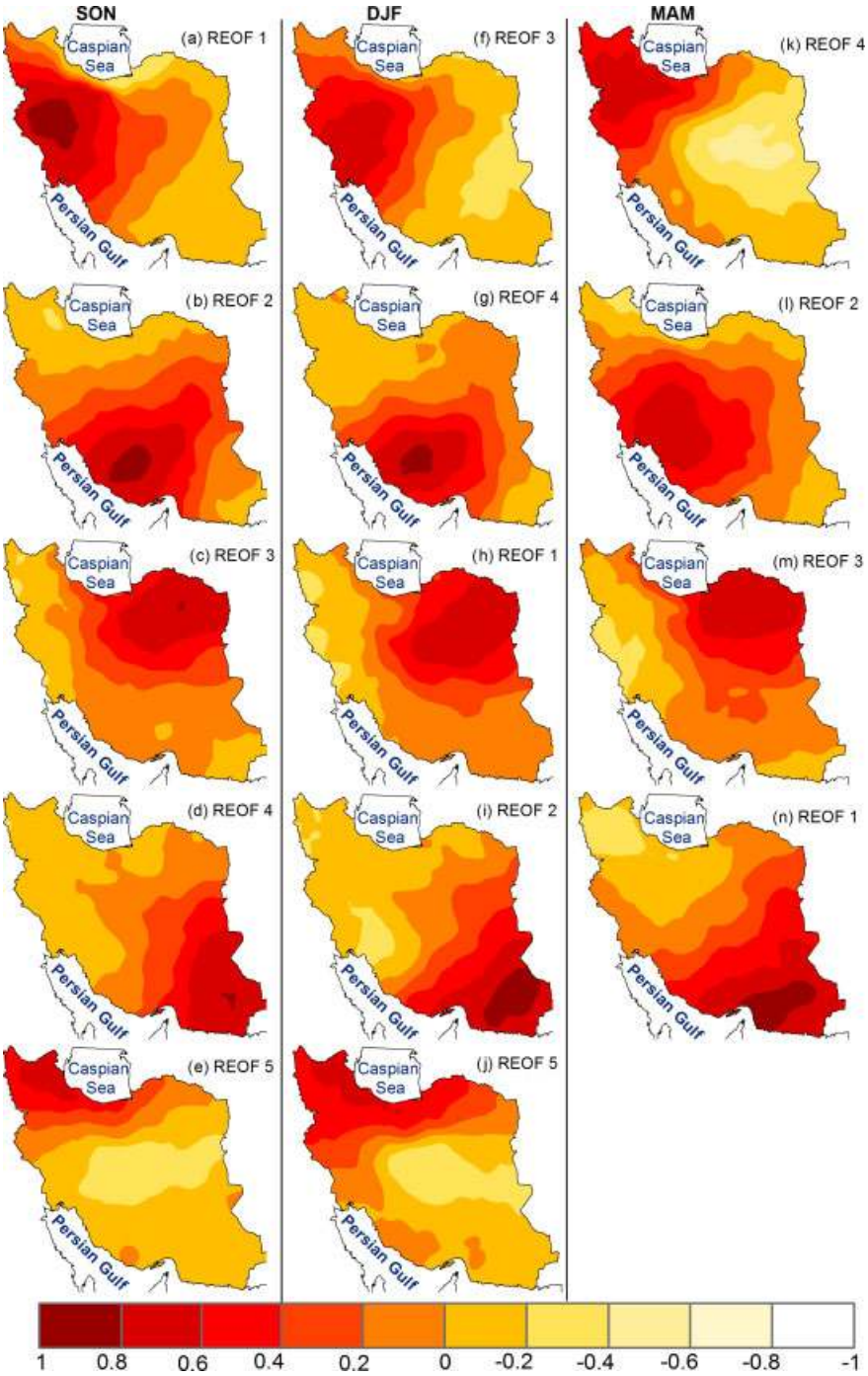

Figure 2. Leading REOFs of daily precipitation over Iran for SON (a)–(e), DJF (f)–(j), and MAM (k)–(n). The rotated spatial patterns are ranked according to the same identified sub-regions rather than the ascending order of the eigenvalues. This figure is available in colour online at wileyonlinelibrary.com/journal/joc

second REOFs represent 14.0 and 13.8% of total variance, respectively, and isolate central-western and southwestern Iran as distinct sub-regions of daily precipitation variability. REOF 3 explains 13.1% of total variance and isolates a sub-region in northeastern Iran. Independent precipitation variability in southeastern and northwestern Iran is represented by REOF 4 and 5, respectively (11.4 and 6.9% of total variance). In DJF, the target area is also divided into five sub-regions of precipitation variability very similar to those previously identified for SON (Figure 2(f)–(j)). In MAM, the four REOFs also show similar sub-regions, but now the central-western and northwestern regions are jointly represented by the first mode (Figure 2(k)–(n)).

3.2. Precipitation regimes and large-scale atmospheric circulation types

In this section, it is first demonstrated that the identified modes of precipitation variability are indeed a manifestation of different PRs. Second, the atmospheric circulation types associated with each PR are dynamically analysed by considering the geopotential height and relative vorticity fields at 500 hPa, as well as the moisture transports and streamlines at 850 hPa. Figure 3 shows the contributions (in percent) of each PR to total seasonal precipitation when only days with RPCs >1.5 are taken into account. A comparison between Figure 2 and Figure 3 reveals a clear agreement between the REOFs and the corresponding contribution patterns, highlighting the regional differentiation achieved through the precipitation modes.

Composite maps of geopotential height and relative vorticity at 500 hPa are shown in Figure 4, while composites of moisture transports and streamlines at 850 hPa are shown in Figure 5. Since compositing is usually known as a circulation typing approach (Yarnal *et al.*, 2001), the composites of the atmospheric fields are also called here circulation types (CTs). In order to facilitate the analysis, the CTs (Figures 4 and 5) are ranked in the same order as the REOFs in Figure 2.

Table II shows the spatial correlation coefficients obtained by projecting all individual daily 500-hPa geopotential height maps of a given season and PR onto the associated composite map. On average, the spatial correlation between individual daily maps and the associated composite for all seasons and regimes is higher than 0.91, reaching values as high as 0.98, revealing strong group similarities. The lowest observed correlations for all seasons and regimes are also presented, though they are still statistically significant at the 99% confidence level ($p < 0.01$). This means that the composite maps of the 500-hPa geopotential height are well representative of the group.

3.2.1. Precipitation regimes in the identified sub-regions

The statistically-based regionalisation here employed does not necessarily imply different PRs in the identified sub-regions. The Varimax rotation allows the identification of sub-regions with largely independent climate variability, as the rotated PC scores (RPCs) are temporally orthogonal (Rencher, 1998). However, the orthogonality of RPCs does not guarantee the existence of different PRs in the sub-regions. One way to objectively describe a PR is the analysis of the empirical distribution of daily precipitation totals in the area of interest. Thus, in order to test if the identified sub-regions are characterized by different PRs, the statistical distributions of area-mean daily precipitation, averaged over grid points with REOF loadings ≥ 0.6, are considered (Figure 2). The two-sample Kolmogorov-Smirnov test is applied to check the null-hypothesis that the distributions are equal. According to the hypothesis testing, all sub-regions are characterized by non-equal distributions, at least at a 99% confidence level ($p < 0.01$), which suggests that their own PRs are very likely to be different.

3.2.2. Precipitation regimes and large-scale circulation during SON, DJF, and MAM

Central-western regime: The percentages of accumulated precipitation shown in Figure 3(a), (f) and (k) depict the highest precipitation amounts in central-western region (during SON and DJF) and northwestern region (during MAM). During SON, the associated CT at 500 hPa highlights that the presence of a deep mid-tropospheric trough over the Middle East (westwards of Iran), associated with a strong positive core in the relative vorticity, is highly favourable to precipitation occurrences in central-western Iran (Figure 4(a)). In the lower troposphere (850 hPa), this PR is accompanied by a cyclone northwestwards of Iraq and an anticyclone southwards (hereafter Arabian anticyclone). These two systems jointly yield moisture transports from the Arabian Sea, Persian Gulf, Red Sea, and eastern Mediterranean towards Iran (Figure 5(a)). Therefore, the combination of high moisture transports at low levels and ascending motions in the cyclonic area explains the development of precipitation events. Owing to the Iranian mountain ranges (Figure 1), these rain-generating mechanisms are enhanced by topographic barrier effects over western Iran and weakened in the respective lee side.

The CT for DJF (Figure 4(f)) is very similar to the corresponding SON pattern (Figure 4(a)). Here, the existence of a 500-hPa-trough axis over Syria and a ridge over the Hormoz Strait leads to strong convergence over western Iran, along the Persian Gulf (Figure 5(f)). Similarly, during MAM the PR is associated with a mid-tropospheric trough over Syria and Jordan (Figure 4(k)); the low-tropospheric Arabian anticyclone and a cyclone in northwestern Iran contribute to moist transports from southern water bodies (Figure 5(k)).

Southwestern regime: For the three seasons, the southwestern region represents an area with a different PR. The percentages of accumulated precipitation (Figure 3(b), (g) and (l)) show the highest precipitation amounts in that region, close to the Persian Gulf. The PR during SON is

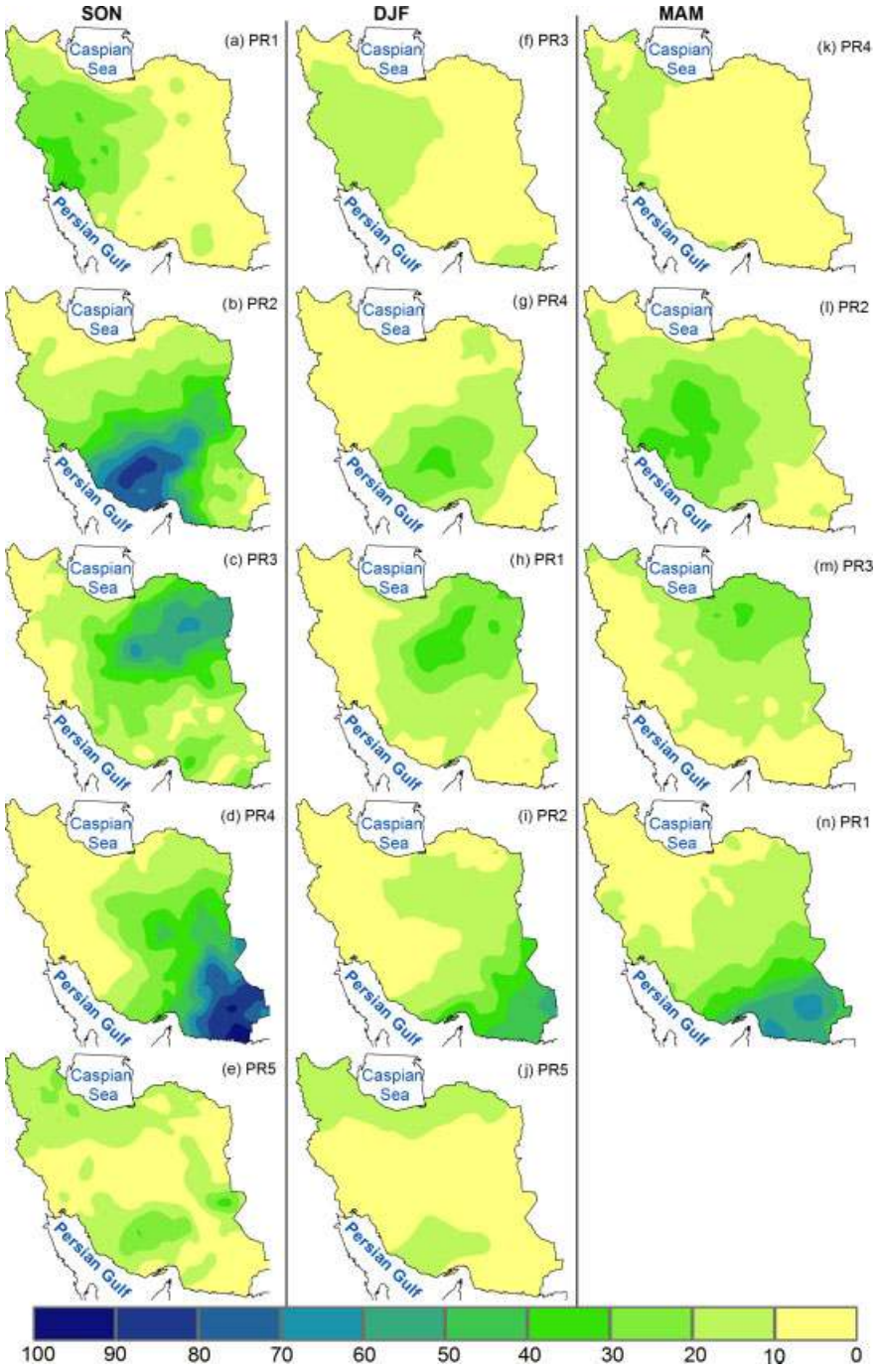

Figure 3. Contributions (in percent) of each precipitation regime (PR) to the total seasonal precipitation for days with RPCs >1.5 in SON (a)–(e), DJF (f)–(j), and MAM (k)–(n). This figure is available in colour online at wileyonlinelibrary.com/journal/joc

associated with a relatively weak mid-tropospheric trough over Iraq (Figure 4(b)). The lower tropospheric flow pattern shows the Arabian anticyclone in eastern Saudi Arabia, which favours moisture transports into southern Iran (Figure 5(b)). Topographic effects further enhance the rain-generating mechanisms in the region.

The 500-hPa pattern for DJF (Figure 4(g)) is similar to its autumn counterpart (Figure 4(b)), especially considering the flow curvature over the area, though they differ in the geopotential gradient (sharper in winter). This pattern can also be distinguished from that in Figure 4(f), mainly due to the displacement of the mid-tropospheric ridge from the Hormoz strait towards the east (Figure 4(g)), yielding a shift in the moisture transports from western to southern Iran (Figure 5(g)).

Also during MAM, the 500-hPa geopotential height pattern shows a wide trough over Syria and Jordan and a ridge over eastern Iran (Figure 4(l)). In the lower troposphere, the Arabian anticyclone over eastern Saudi Arabia induces moisture transports from the southern water bodies to western Iran, leading to precipitation (Figure 5(l)).

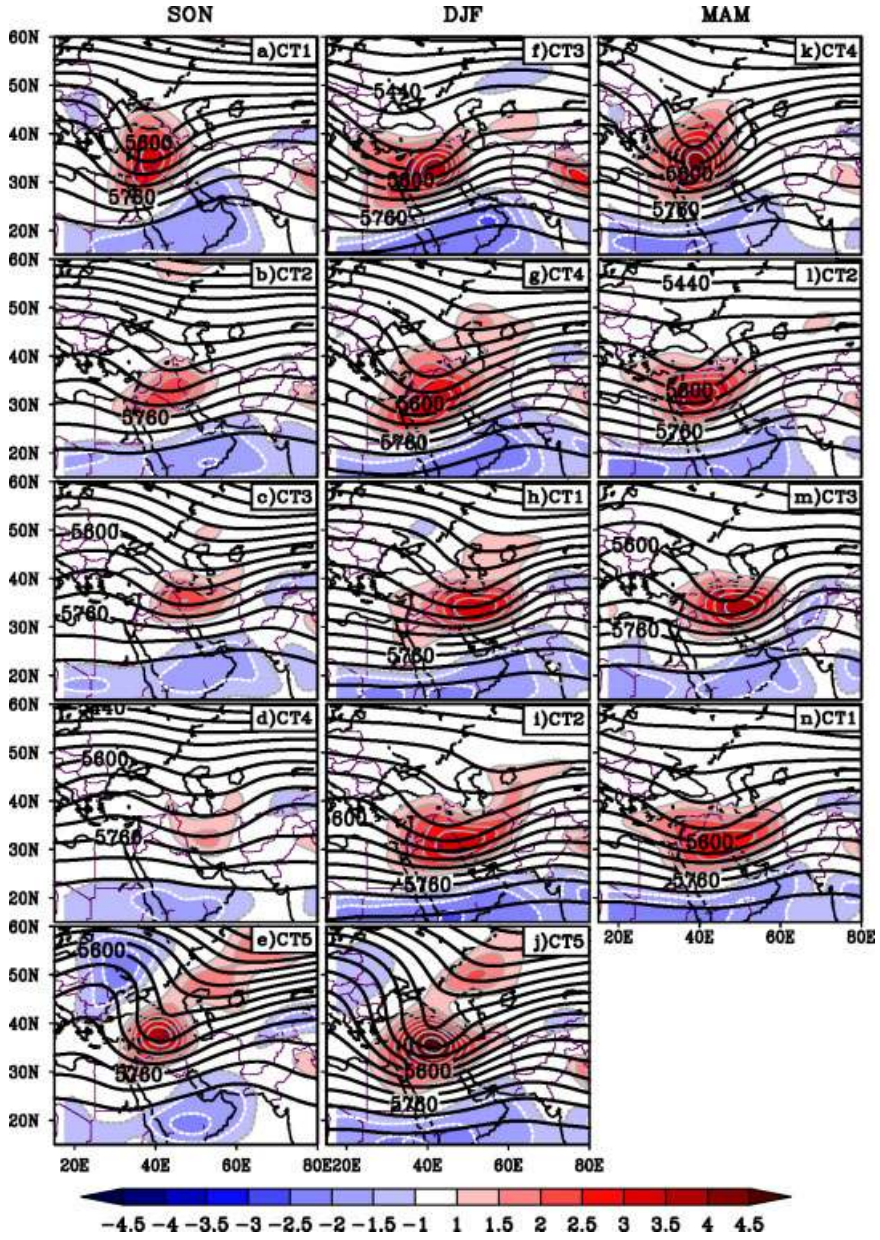

Figure 4. Circulation types (CTs): composites of the 500-hPa geopotential height (contours in gpm) and 500-hPa relative vorticity (shading in 10^{-5} s^{-1}; dashed lines indicate negative vorticity) associated with the precipitation regimes (PRs) in SON (a)–(e), DJF (f)–(j), and MAM (k)–(n). This figure is available in colour online at wileyonlinelibrary.com/journal/joc

Northeastern regime: During SON the PR in the northeastern region (Figure 3(c)) is related to a trough with its axis over the Caspian Sea (Figure 4(c)). The mid-tropospheric cyclonic circulation is accompanied by a low-tropospheric anticyclonic circulation southwards of Iran, which enables the incursion of moisture transports into eastern Iran (Figure 5(c)), a region often sheltered by topography.

During DJF the 500-hPa geopotential height pattern (Figure 4(h)) is similar to the corresponding SON pattern (Figure 4(c)), but the main trough is now southwardly displaced and the positive vorticity area is much wider and stronger. Additionally, a ridge located over Pakistan is further enhanced when compared to autumn, which in turn strengthens the low-tropospheric anticyclonic circulation producing large-scale convergence and precipitation over northeastern and southern Iran. The Mediterranean Sea and the Persian Gulf appear to be the main moisture sources for this regime (Figure 5(h)).

Similarly, during MAM a mid-tropospheric trough over western Iran (Figure 4(m)) is connected in the lower troposphere to a cyclonic system in northeastern Iran and to the Arabian anticyclone over the Arabian Sea (Figure 5(m)).

Southeastern regime: During SON the percentages of accumulated precipitation in southeastern area reach values above 90% (Figure 3(d)), which is a significant precipitation amount comparable to that occurring in the southwestern part of the country during the same season

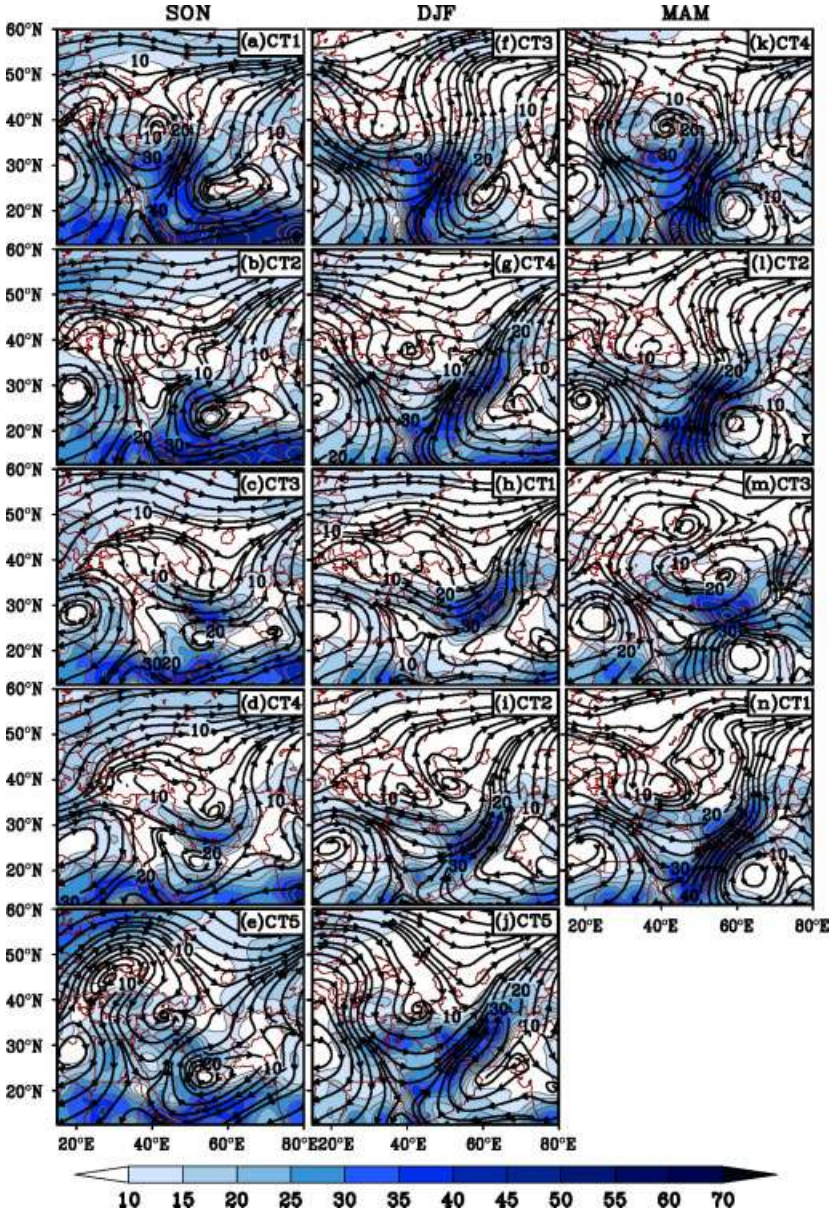

Figure 5. Circulation types (CTs): composite maps of moisture transport (g s^{-1}) and streamlines at 850 hPa associated with the precipitation regimes (PRs) in SON (a)–(e), DJF (f)–(j), and MAM (k)–(n). This figure is available in colour online at wileyonlinelibrary.com/journal/joc

Table II. Spatial correlation coefficients between individual daily 500-hPa geopotential height maps of a given season and precipitation regime (PR), and the associated composite map. The lowest, mean, and highest correlations are listed.

Season	Correlation Coefficient	PR1	PR2	PR3	PR4	PR5
SON	Lowest	0.83	0.75	0.74	0.80	0.67
	Mean	0.92	0.91	0.92	0.90	0.93
	Highest	0.98	0.98	0.99	0.98	0.98
DJF	Lowest	0.81	0.83	0.79	0.83	0.80
	Mean	0.94	0.93	0.93	0.93	0.93
	Highest	0.98	0.98	0.99	0.98	0.99
MAM	Lowest	0.80	0.75	0.70	0.77	
	Mean	0.92	0.92	0.91	0.92	
	Highest	0.99	0.98	0.98	0.99	

(Figure 3(b)). This regime is characterized by a weak mid-tropospheric trough over Iran (Figure 4(d)). In the lower troposphere, there is a cyclonic circulation over Iran and the Arabian anticyclone over Saudi Arabia, both acting to provide moisture and precipitation over the southern regions (Figure 5(d)).

The 500-hPa pattern during DJF is characterized by a trough in western Iran (Figure 4(i)); in the lower troposphere, there is a convergence of moisture transports over southeastern Iran, apparently coming from the southern water bodies and from the Mediterranean (Figure 5(i)).

During MAM the 500-hPa geopotential height pattern features a wide trough, with associated positive vorticity over Iraq and western Iran, followed by a broad ridge over Pakistan and Afghanistan (Figure 4(n)). This CT depicts the low-tropospheric Arabian anticyclone over the Arabian Sea that favours moisture transports from the

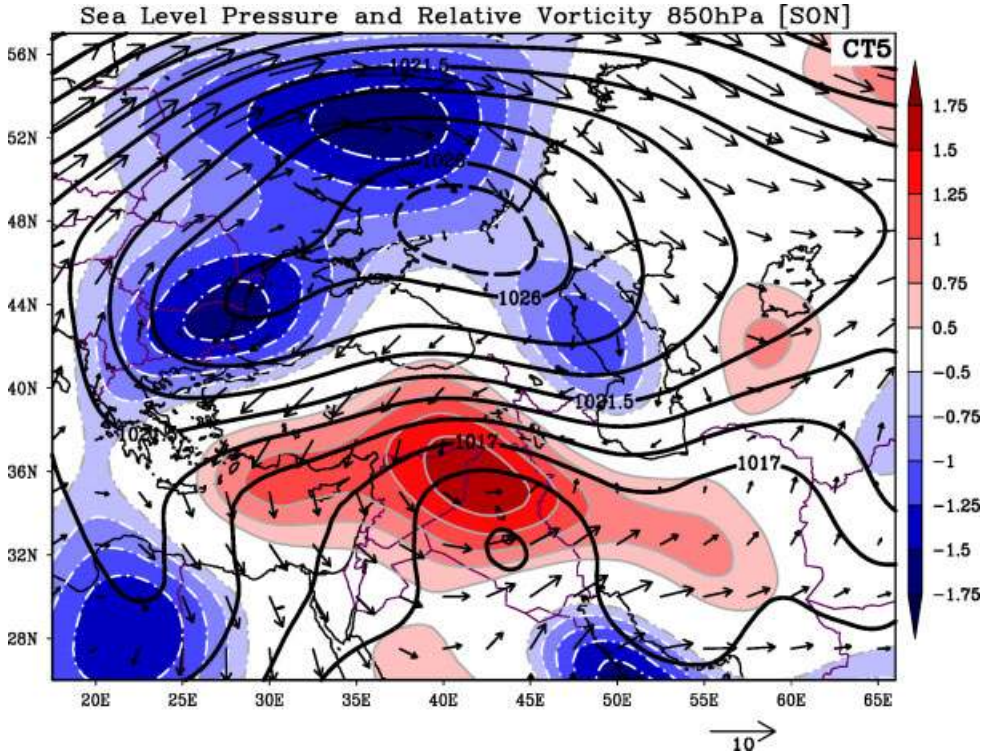

Figure 6. Mean sea level pressure field (solid contours in hPa), relative vorticity (filled contours in 10^{-5} s^{-1}; Solid and dot-dashed lines indicate positive and negative vorticity, respectively) and horizontal wind vectors at 850 hPa for the 'Caspian Sea precipitation regime' in SON (Figure 2e). This figure is available in colour online at wileyonlinelibrary.com/journal/joc

southern water bodies to southeastern Iran (Figure 5(n)). The location of this anticyclone in the easternmost part of the Arabian Sea, with the associated 500-hPa ridge over Pakistan and Afghanistan, are the main large-scale factors underlying the convergence of moist air and resulting precipitation occurrences in southeastern Iran.

Northwestern (Caspian Sea) regime: Even though the northwestern spatial mode during SON is dominant for precipitation occurrence in the Caspian Sea region (Figure 2(e)), its precipitation contribution shows a less clear pattern (Figure 3(e)), with other noticeable contributions over Iran. The 500-hPa geopotential height pattern shows a positive vorticity core and a deep trough extending from eastern Turkey towards the Caspian Sea (Figure 4(e)). The existence of a strong anticyclone located between the Black Sea and the Caspian Sea provides permanent northerly winds over the Caspian Sea, resulting in moisture convergence and precipitation occurrence over the area (Figure 5(e)). This is better illustrated in Figure 6, showing the mean sea level pressure, the relative vorticity and wind vectors at 850 hPa for this 'Caspian Sea precipitation regime'. The convergence of moist northerly flow, generated by the anticyclone located over the western Caspian Sea, with southerly flow, induced by a cyclone over eastern Turkey, usually lead to precipitation in the Caspian Sea area.

During DJF, the mid- and low-tropospheric circulation for this regime (Figure 4(j) and 5(j)) are very similar to their autumn counterparts, though in winter the trough is deeper than in autumn and southwardly displaced. Lastly, it is worth noting the absence of the 'Caspian Sea regime' in spring, when four regimes have been found, since the central-western and northwestern regimes seem to be jointly represented by the first one (Figures 2(k) and 3(k)).

3.3. Role of the Arabian anticyclone in Iranian precipitation regimes

Circulation types displayed in Figure 5 illustrate the anticyclonic circulation over the Arabian Sea, which is responsible for providing moisture for the cyclones developing westwards or northwards of the Arabian anticyclone. Figure 7 further demonstrates the role of the Arabian anticyclone in controlling the spatial pattern of precipitation over Iran, since the location of the Arabian anticyclone (negative vorticity peak in Figure 7) can be considered as an index for determining the location of precipitation occurrence over Iran. Results suggest that precipitation is very likely to occur in the eastern half of Iran (southeastern and northeastern PRs), when the Arabian anticyclone is located at roughly 60–62.5 °E and the anticyclonic circulation over the northern Arabian Sea is weakened (CT1 and CT2 in Figure 7(b) and CT1 and CT3 in Figure 7(c)). Conversely, when the Arabian anticyclone is located within the longitude belt of 52.5–57.5 °E, it tends to favour precipitation occurrences over western Iran. In other words, the displacement of the Arabian anticyclone westwards of its mean position favours precipitation occurrences in western Iran, while

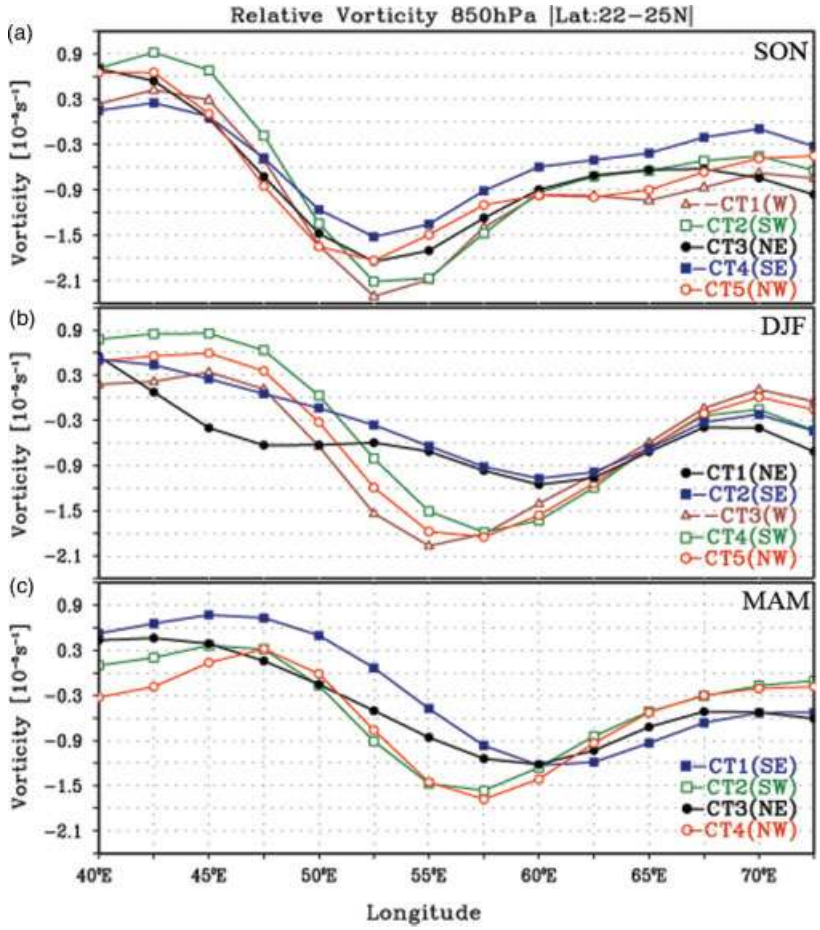

Figure 7. Composites of the relative vorticity at 850 hPa meridionally averaged over 22 °N–25 °N for the different circulation types (CTs) and for: (a) SON, (b) DJF, and (c) MAM. This figure is available in colour online at wileyonlinelibrary.com/journal/joc

its eastward displacement is more favourable to precipitation in eastern Iran.

In fact, the Arabian anticyclone, as a semi-stationary and regional-scale feature, plays a leading role in feeding cyclones over Iran with moisture from the southern water bodies (Figure 5). Exceptions are autumn CT3 and CT4, for which moisture is generally transported from the Persian Gulf and Oman Sea, since the Arabian anticyclone is westwards of its winter-mean position. In autumn, when cyclone tracks are at higher latitudes and the Arabian anticyclone is still at its summer-mean position, the moisture transport axis is northwards of the Arabian Peninsula (Figsure 5(a)–(e) and Figure 7(a)). In winter and spring, the Arabian anticyclone moves to the east and over the Arabian Sea (Figure 5(f)–(n) and Figure 7(b) and (c)).

The importance of the influence of the Arabian anticyclone on Iranian precipitation might be further underlined if one considers that all the identified sub-regions receive more than 80% of their total annual precipitation in December–March, when the Arabian anticyclone is more connected to the Iranian precipitation. Therefore, the presence of the Arabian anticyclone and its specific position over the Arabian Sea largely explains the mechanisms leading to moisture transport into the identified sub-regions in winter and spring.

4. Conclusions and discussion

Seasonal regimes of daily precipitation are identified in Iran by applying PCA with Varimax rotation to a subset of daily precipitation events; as the present study is focused on PRs, in order to discard irrelevant information, only days when at least 10% of all grid points covering Iran present precipitation totals $\geq$5 mm were selected. This analysis is undertaken for three seasons separately (SON, DJF, MAM), excluding summer. The large-scale atmospheric circulation types related to each PR are identified and analysed by compositing daily atmospheric fields for RPC $\geq$1.5.

In autumn and winter, Iran is divided into 5 PRs, with their corresponding modes cumulatively accounting for about 59% of total variance; in spring, four PRs (55% of variance) are identified (Figure 2). Patterns of precipitation contributions isolate similar sub-regions in autumn and winter (northeastern, southeastern, southwestern, central-western, and northwestern, including the Caspian Sea); in spring, it seems that the latter two sub-regions are merged in a single sub-region (Figure 3).

The study suggests that the spatial distribution of precipitation over Iran is mainly governed by large-scale circulation types and, in particular, by the geographical position of the mid-tropospheric troughs/ridges and of

the low-tropospheric Arabian anticyclone. Precipitation occurrence over western Iran is particularly favoured when a trough extends over the eastern Mediterranean to Iraq, whereas, precipitation is very likely to occur in the eastern half of the country when a trough and a ridge are located over western Iran and Pakistan, respectively. These results are in close agreement with the findings of Alijani (2002) and Raziei *et al*. (2011), as they also suggested that the closer the troughs are to Iran the higher the precipitation amounts are over the country. The occurrence of precipitation in Iran, in fact, is due to the interaction between a mid-tropospheric trough over the Middle East and a lower level anticyclone over an area around the Arabian Peninsula and the Arabian Sea. The trough, as a pre-conditioning factor, can provide regional-scale ascending motions, whilst the Arabian anticyclone can transport moisture from southern water bodies into the cyclonic systems.

Precipitation over the Middle East and Iran is usually related to moist air masses originated in the Mediterranean Sea that are advected by the Mediterranean cyclones to the region (e.g. Taha *et al*., 1981; Alijani and Harman, 1985). However, with the exception of the study of Elguindi and Giorgi (2006), which supports this traditional perspective, most recent studies recognized that the southern water bodies (Arabian sea, Oman sea, Persian Gulf, Red sea, and north Indian ocean) are the main moisture sources for Iranian precipitation (Chakraborty *et al*., 2006; Evans and Smith, 2006). In line with these findings, the present results give evidence for the central role played by these water bodies in acting as main moisture sources for Iranian precipitation. Also, the outcomes of some regional studies support the importance of the role played by the Arabian anticyclone in providing moisture for precipitation occurrence over the Middle East and Iran (Krichak and Alpert, 1998; Farajzadeh *et al*., 2007).

The present results suggest that a few CTs contribute to the occurrence of most of the precipitation events in the identified sub-regions. However, the rain-generating CTs differ from one season to the other, even if some common features are detectable. The occurrence of some PRs is indeed of crucial importance for the precipitation predictability at regional scale. In order to improve the representation of orographic precipitation patterns, the APHRO_V0902 precipitation dataset employs a dense network of rain-gauge data over Asia, including mountainous areas such as the Himalayas and Zagros (Iran), where the most important water resources for the Asian environment are located (Yatagai *et al*., 2009). However, further efforts should be undertaken to validate the identified relationships with other sources of data (different gridded datasets or re-analysis). It is also of great interest to test the potential predictability of the precipitation events using the identified CTs (for example by applying multiple linear regression models). Finally, the methodology here developed can be applied to other extratropical regions, where large-scale atmospheric forcing tends to play a key role in triggering precipitation.

Acknowledgements

NCEP/NCAR data was provided by the NOAA-CIRES Climate Diagnostics Center, Boulder, Colorado, USA (http://www.cdc.noaa.gov). APHRO_V0902 gridded daily precipitation data was provided by the Research Institute for Humanity and Nature of Japan, http://www.chikyu.ac.jp/precip. We also thank the anonymous reviewers for their valuable comments.

References

Alijani B. 2002. Variation of 500 hPa flow patterns over Iran and surrounding areas and their relationship with climate of Iran. *Theoretical and Applied Climatology* **72**: 41–54.

Alijani B, Harman JR. 1985. Synoptic climatology of precipitation in Iran. *Annals of the Association of American Geographers* **75**(3): 404–416.

Bogardi I, Matyasovszky I, Bardossy A, Duckstein L. 1994. A hydroclimatological model of areal drought. *Journal of Hydrology* **153**: 245–264.

Bonell M, Sumner G. 1992. Atmospheric Circulation and Daily Precipitation in Wales. *Theoretical and Applied Climatology* **46**: 3–25.

Chakraborty A, Behera SK, Mujumdar M, Ohba R, Yamagata T. 2006. Diagnosis of tropospheric moisture over Saudi Arabia and influences of IOD and ENSO. *Monthly Weather Review* **134**: 598–617.

Chen M, Xie P, Janowiak JE, Arkin PA. 2002. Global land precipitation: a 50-year monthly analysis based on gauge observations. *Journal of Hydrometeorology* **3**: 249–266.

Corte-Real J, Qian B, Xu H. 1998. Regional climate change in Portugal: precipitation variability associated with large-scale atmospheric circulation. *International Journal of Climatology* **18**: 619–635.

Dinpashoh Y, Fakheri-Fard A, Moghaddam M, Jahanbakhsh S, Mirnia M. 2004. Selection of variables for the purpose of regionalization of Iran's precipitation climate using multivariate methods. *Journal of Hydrology* **297**: 109–123.

Domroes M, Kaviani M, Schaefer D. 1998. An analysis of regional and intra-annual precipitation variability over Iran using multivariate statistical methods. *Theoretical and Applied Climatology* **61**: 151–159.

Elguindi N, Giorgi F. 2006. Simulating multi-decadal variability of Caspian Sea level changes using regional climate model outputs. *Climate Dynamics* **26**: 167–181.

Esteban-Parra MJ, Rodrigo FS, Castro-Diez Y. 1998. Spatial and temporal patterns of precipitation in Spain for the period 1880–1992. *International Journal of Climatology* **18**: 1557–1574.

Evans JP, Smith RB. 2006. Water vapor transport and the production of precipitation in the eastern fertile crescent. *Journal of Hydrometeorology* **7**: 1295–1307.

Farajzadeh M, Karimi M, Ghaemi H, Mobasheri MR. 2007. Studying the moisture flux over west of Iran. *Journal of Applied Sciences* **7**: (20): 3023–3030.

Fovell RG, Fovell MY. 1993. Climate zones of the conterminous United States defined using cluster analysis. *Journal of Climate* **6**: 2103–2135.

Frakes B, Yarnal B. 1997. A procedure for blending manual and correlation-based synoptic classifications. *International Journal of Climatology* **17**: 1381–1396.

Ghasemi AR, Khalili D. 2008. The association between regional and global atmospheric patterns and winter precipitation in Iran. *Atmospheric Research* **88**: 116–133.

Kidson JW. 2000. An analysis of New Zealand synoptic types and their use in defining weather regimes. *International Journal of Climatology* **20**: 299–316.

Kistler R, Kalnay E, Collins W, Saha S, White G, Woollen J, Chelliah M, Ebisuzaki W, Kanamitsu M, Kousky V, van den Dool H, Jenne R, Fiorino M. 2001. The NCEP/NCAR 50-Year Reanalyses: monthly means CD-ROM and documentation. *Bulletin of the American Meteorological Society* **82**: 247–268.

Kostopoulou E, Jones PD. 2007. Comprehensive analysis of the climate variability in the eastern Mediterranean. Part I: Map pattern classification. *International Journal of Climatology* **27**: 1189–1214.

Krichak S, Alpert P. 1998. Role of large Scale moist dynamics in November 1–5, 1994 hazardous Mediterranean Weather. *Journal of Geophysical Research* **103**(16): 19453–19468.

Lamb HH. 1977. *Climate, present, past and future. (vol. 2) Climate history and the future*. Methuen: London.

Nazemosadat MJ, Cordery I. 2000. On the relationships between ENSO and autumn rainfall in Iran. *International Journal of Climatology* **20**: 47–61.

Nazemosadat MJ, Ghasemi AR. 2004. Quantifying the ENSO-related shifts in the intensity and probability of drought and wet periods in Iran. *Journal of Climate* **17**: 4005–4018.

Neal RA, Phillips ID. 2009. Summer daily precipitation variability over the East Anglian region of Great Britain. *International Journal of Climatology* **29**: 1661–1679.

North GR, Bell TL, Cahalan RF. 1982. Sampling errors in the estimation of empirical orthogonal functions. *Monthly Weather Review* **110**: 699–706.

Raziei T, Bordi I, Pereira LS. 2008. A precipitation-based regionalization for Western Iran and regional drought variability. *Hydrology and Earth System Sciences* **12**: 1309–1321.

Raziei T, Bordi I, Pereira LS, Corte-Real J, Santos JA. 2011. Relationship between daily atmospheric circulation types and winter dry/wet spells in western Iran. *International Journal of Climatology* DOI: 10.1002/joc.2330.

Raziei T, Saghafian B, Paulo AA, Pereira LS, Bordi I. 2009. Spatial patterns and temporal variability of drought in western Iran. *Water Resources Management* **23**: 439–455.

Rencher AC. 1998. *Multivariate statistical inference and applications*. Wiley: Hoboken.

Richman MB. 1986. Rotation of principal components. *International Journal of Climatology* **6**: 293–335.

Romero R, Sumner G, Ramis C, Genoves C. 1999. A classification of the atmospheric circulation patterns producing significant daily rainfall in the Spanish Mediterranean area. *International Journal of Climatology* **19**: 765–785.

Santos JA, Corte-Real J, Leite SM. 2005. Weather regimes and their connection to the winter rainfall in Portugal. *International Journal of Climatology* **25**: 33–50.

Serrano A, García JA, Mateos VL, Cancillo M L, Garrido J. 1999. Monthly modes of variation of precipitation over the Iberian Peninsula, *Journal of Climate* **12**: 2894–2919.

Shepard D. 1968. A two-dimensional interpolation function for irregularly spaced data, Proc. 23 ACM Nat'l Conf., Princeton, NJ, Brandon/Systems Press, 517–524.

Soltani S, Modarres R, Eslamian SS. 2007. The use of time series modelling for the determination of rainfall climates of Iran. *International Journal of Climatology* **27**: 819–829.

Taha MF, Harb SA, Nagib MK, Tantawy AH. 1981. The climate of the Near East. In: *Climates of Southern and Western Asia: World Survey of Climatology*, Takahashi K, Arakawa H (eds). Vol. 9. Elsevier: Amsterdam.

Wibig J. 1999. Precipitation in Europe in relation to circulation patterns at the 500 hPa level. *International Journal of Climatology* **19**: 253–269.

Xoplaki E, Luterbacher J, Burkard R, Patrikas I, Maheras P. 2000. Conection between the large-scale 500 hPa geopotential height field and precipitation over Greece during wintertime. *Climate Research* **14**: 129–146.

Yarnal B, Comrie AC, Frakes B, Brown DP. 2001. Developments and prospects in synoptic climatology. *International Journal of Climatology* **21**: 1923–1950.

Yatagai A, Arakawa O, Kamiguchi K, Kawamoto H, Nodzu MI, Hamada A. 2009. A 44-year daily gridded precipitation dataset for Asia based on a dense network of rain gauges. *SOLA* **5**: 137–140.

Yatagai A, Xie P, Alpert P. 2008. Development of a daily gridded precipitation data set for the Middle East. *Journal of Advances in Geosciences* **12**: 165–170.

